Powder Technology 366 (2020) 488–496

Contents lists available at ScienceDirect

Powder Technology

journal homepage: www.elsevier.com/locate/powtec

The hopper angle role on the velocity and solid-fraction profiles at the outlet of silos

J.R. Darias [a,b], D. Gella [a], M.E. Fernández [c], I. Zuriguel [a], D. Maza [a,*]

[a] Departamento de Física y Matemática Aplicada, Facultad de Ciencias, Universidad de Navarra, Pamplona, Spain
[b] Laboratorio de Óptica y Fluidos, Universidad Simón Bolivar, Apart. Post. 89000, Caracas 1080-A, Venezuela
[c] Dept. Ing. Mecánica, Fac. Reg. La Plata, Univ. Tecnológica Nacional, Av. 60 Esq 124, RA-1900 La Plata, Buenos Aires, Argentina

ARTICLE INFO

Article history:
Received 4 December 2019
Received in revised form 28 January 2020
Accepted 24 February 2020
Available online 25 February 2020

Keywords:
Hoppers
Mass flow rate
Silos discharge dynamics

ABSTRACT

Hoppers are one of the most popular devices implemented to allow precise flow control mechanism when dispensing granulate materials from silos and other containers. Despite its ubiquity in many industrial processes, the effect that hopper geometry has on the flow rate is still poorly understood. In this work, we study the influence of the hopper angle on the main two variables that determine the flow rate: the solid-fraction and the velocities of the particles. To this end, we use a quasi-two-dimensional system which allows a precise characterization of the profiles of these variables at the orifice. Using these experimental results, we compute the flow-density vector and obtain the resulting expression for the volumetric flow rate. Finally, we compare this expression with an equation introduced back in 1961 by RL Brown.

1. Introduction

One of the most common procedures implemented in any industrial process is the delivery of grains through orifices. Such a situation provides a simple mechanism to distribute, mix or manipulate raw or processed materials in a large variety of practical scenarios [2]. Despite its apparent simplicity, a large number of technical problems must be carefully attended to guarantee the correct operation of these devices. Although the easiest and straightforward method to control the delivered mass is to modify the exit size, there are other parameters, like the hopper angle, that can be easily adjusted in practice. Nevertheless, we still lack a true mathematical expression relating flow rate, outlet size and hopper angle. Even the prediction of the most straightforward case –the flow rate corresponding to a flat bottom silo – is not entirely understood in terms of micromechanical variables. Early in the sixties, Beverloo et al. [3] proposed the most commonly used expression that correlates flow rate and outlet size for bunkers:

$$W = C\rho_B\sqrt{g}(D-kd)^{5/2} \tag{1}$$

where $\rho_B = \rho_M\phi_B$ is the bulk density (i.e. the particle material density ρ_M times the bulk volume fraction ϕ_B), D is the exit orifice diameter, d the typical grain size and C, k are fitting parameters.

The arguments used by Beverloo (initially introduced by Hagen in 1852 [4] and subsequently rephrased by Nedderman [5]) assumed that the grains exit velocity scales with the outlet size as $\sqrt{D}$. Whereas the fitting parameter C in Eq. 1 seems to be related with the material properties (such as the friction coefficient), the role of k is more subtle. This parameter - introduced by Brown and Richards in 1970 [6] - is connected with the idea that particles, when flowing through the outlet, can not approach the border beyond a specific scale kd, determining in consequence an effective outlet size of diameter $(D - kd)$.

At the beginning of this century, Mancok et al. [7] introduced a new expression inspired in these previous works:

$$W = C'\rho_o\left[1-\alpha_1 e^{-D'/\alpha_2}\right]\sqrt{g}(D'-1)^{5/2} \tag{2}$$

In this equation, the outlet size is normalized by the particle typical diameter, $D' = D/d$, and the k parameter is excluded. The authors also suggest that the apparent density of the material at outlet neighborhood, ρ_o, depends on the orifice size and does not match with the bulk density, i.e. $\rho_o < \rho_B$.

More recently, Janda et al. [8] developed an alternative approach based on the of velocity and solid-fraction profiles measured at the outlet of a quasi-2D silo. In that work, it was shown that these profiles are self-similar when are rescaled with their values at the exit centre. Expressions proposed to describe these magnitudes at the 2D-silo exit are:

* Corresponding author.
E-mail address: dmaza@unav.es (D. Maza).

https://doi.org/10.1016/j.powtec.2020.02.061
0032-5910/

$$v(x) = \sqrt{2g\gamma R}\ \left[1-(x/R)^2\right]^a \tag{3}$$

$$\phi(x) = \phi_\infty\left(1-\alpha_1 e^{-R/\alpha_2}\right)\ \left[1-(x/R)^2\right]^b = \phi_c\ \left[1-(x/R)^2\right]^b \tag{4}$$

and consequently, the flow rate will be given by:

$$W = C''\rho_M\phi_c\sqrt{\gamma g}R^{3/2} \tag{5}$$

where $C'' = \sqrt{2}\beta\left(\frac{1}{2}, 1+[a+b]\right)$ with the β-function, defining the horizontal dependence of the flow-density profile through the parameters a and b; ϕ_c is the volume fraction at the exit centre and γ quantifies the particle acceleration along the container vertical axis [9]. In particular γ coefficient is defined as the integral of the normalized acceleration, $a(z)/g$, along the normalized coordinate, $h = z/R$:

$$\gamma = \int_0^\infty \frac{a(z)}{g}dh \tag{6}$$

Similar ideas were posteriorly implemented by other authors to reproduce the silo flow rate in different scenarios [10]. Importantly, the role of γ has been proved to be also useful to describe polydisperse systems [11,12] Apart from these two expressions, other correlations between the outlet size an the mass flow rate have been proposed; an exhaustive list of them can be found in [13].

Let us now revise some of the arguments historically used to include the hopper angle role in the flow rate expression. In 1960, R.L. Brown and J.C. Richards [1,6] imagined the existence of a surface above the outlet from which the grains fall only under the gravity action, naming it *free fall arch*. Hence, their analysis provided a practical framework to integrate the material flow-density leading to an expression for the discharge rate. Two relevant assumptions were used to do that: a) the free fall arch has spherical symmetry and b) the material apparent

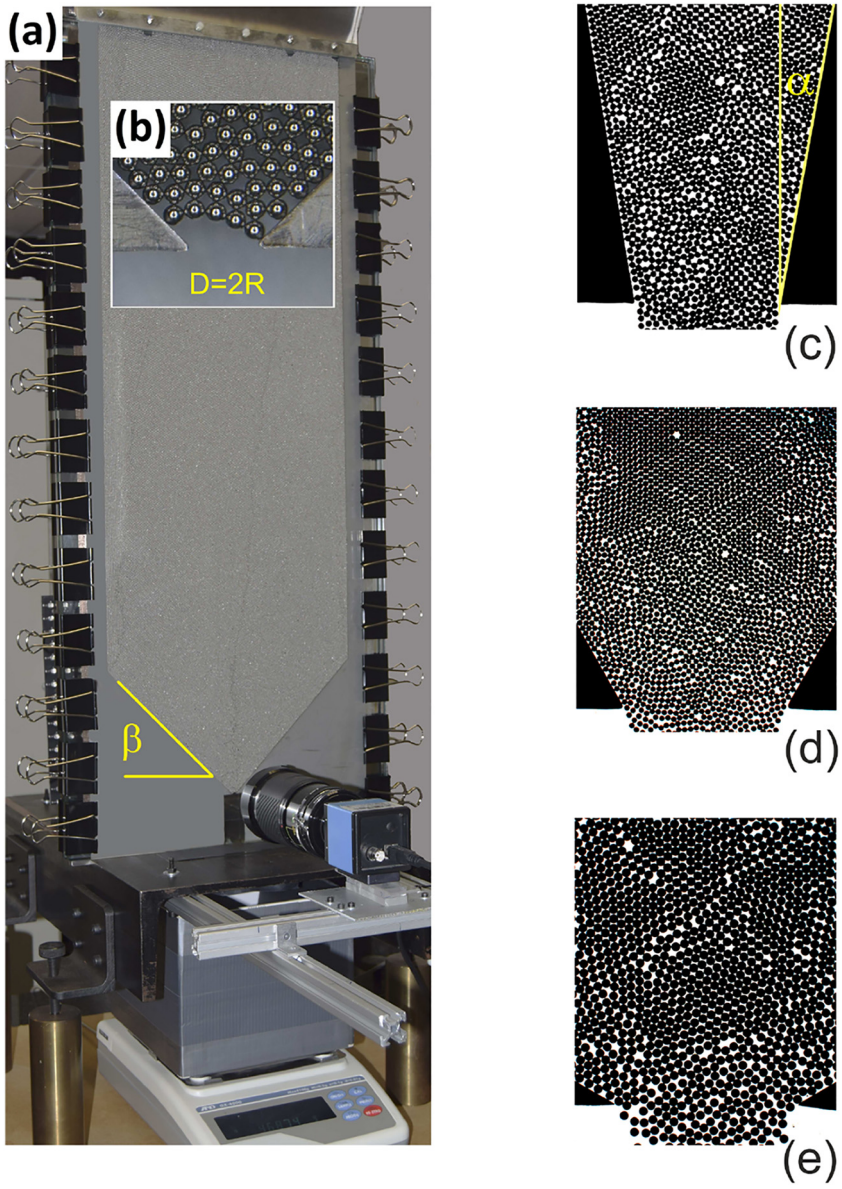

Fig. 1. Experimental setup: (a) Half million of steel beads ($d = 0.1\,cm$) are contained in a quasi 2D silo conforming a single vertical layer. The discharge takes place through a hopper at the bottom. (b) Detail of the outlet which size is characterized by $D = 2R$. In this case, the aperture is small ($D = 3.5d$) and a clogging event could eventually occur. The three hopper angles explored in this work, (c) $\alpha = 10^{\circ}$, (d) $\alpha = 30^{\circ}$, (e) $\alpha = 60^{\circ}$.

density near the outlet region is invariant and coincides with the bulk density. Accordingly, the angular dependence of the velocity field at such hypothetical surface can be calculated under the *Minimum Energy* postulate [1], resulting in the volumetric flow rate expression:

$$Q^{BR}(\alpha) = \left[\frac{\pi}{6}\frac{(1-\cos^{3/2}\alpha)}{\sin^{5/2}\alpha}\right]\phi_B\sqrt{g}(D-kd)^{5/2} \tag{7}$$

for a cylindrical hopper, and

$$Q^{BR}(\alpha) = \left[\frac{\int_0^\alpha \sqrt{\cos\theta}\,d\theta}{\sin^{3/2}\alpha}\right]\phi_B\sqrt{2g}l(D-kd)^{3/2} \tag{8}$$

for a 2D silo. Here, θ is the cenital coordinate, α is the hopper angle, and l is the layer depth. Let us mention that Nedderman used a similar approach, named by him *Hour Glass Theory* [5], introducing a formal relationship between the angular and radial stress directions inside the hopper. However, we will not further develop this idea here as this approach is unpractical for the 2D case.

In this work, inspired by Brown&Richards approach, we investigate the hopper angle effect on the velocity and solid-fraction profiles, and consequently, on the flow rate. Apart from the flat bottomed case, three other representative hopper angles are studied to unveil the effect of this variable on velocity and solid-fraction. The election of these angles is founded in the predictions of Eq. 8.

2. Experimental setup

The setup is approximately the same used in previous experiments [8,9,14] where a single layer of monodisperse steel spherical beads (0.1 cm diameter) was discharged through an central slit of width D in the base of a flat silo. In this case, the silo has been constructed sandwiching 0.1 cm stainless steel sheets between 1 cm thick glass panels. As the sheets determine the gap between glass boundaries, we have supplemented them with aluminum foils of 0.01 cm thickness to mitigate lateral friction effects on the beads. In order to fix the hopper angle, the sheets have been cut by a precision laser cutting machine. Fig. 1 shows an entire view of the experimental setup and a detail of the hopper used. In this work, we report the results corresponding to three different hopper angles, $\alpha = 10°\alpha = 30°$ and $\alpha = 60°$ besides of the flat bottom silo, $\alpha = 90°$. Note that in a previous work [14], with the same experimental setup, the wall tilt angle, $\beta = \frac{\pi}{2} - \alpha$, was used to characterize the hopper inclination. Nevertheless, here we will use the established technical notation of the "hopper angle" (or "hopper half angle" [15]) as the angle defined between the vertical direction and the tilted exit wall.

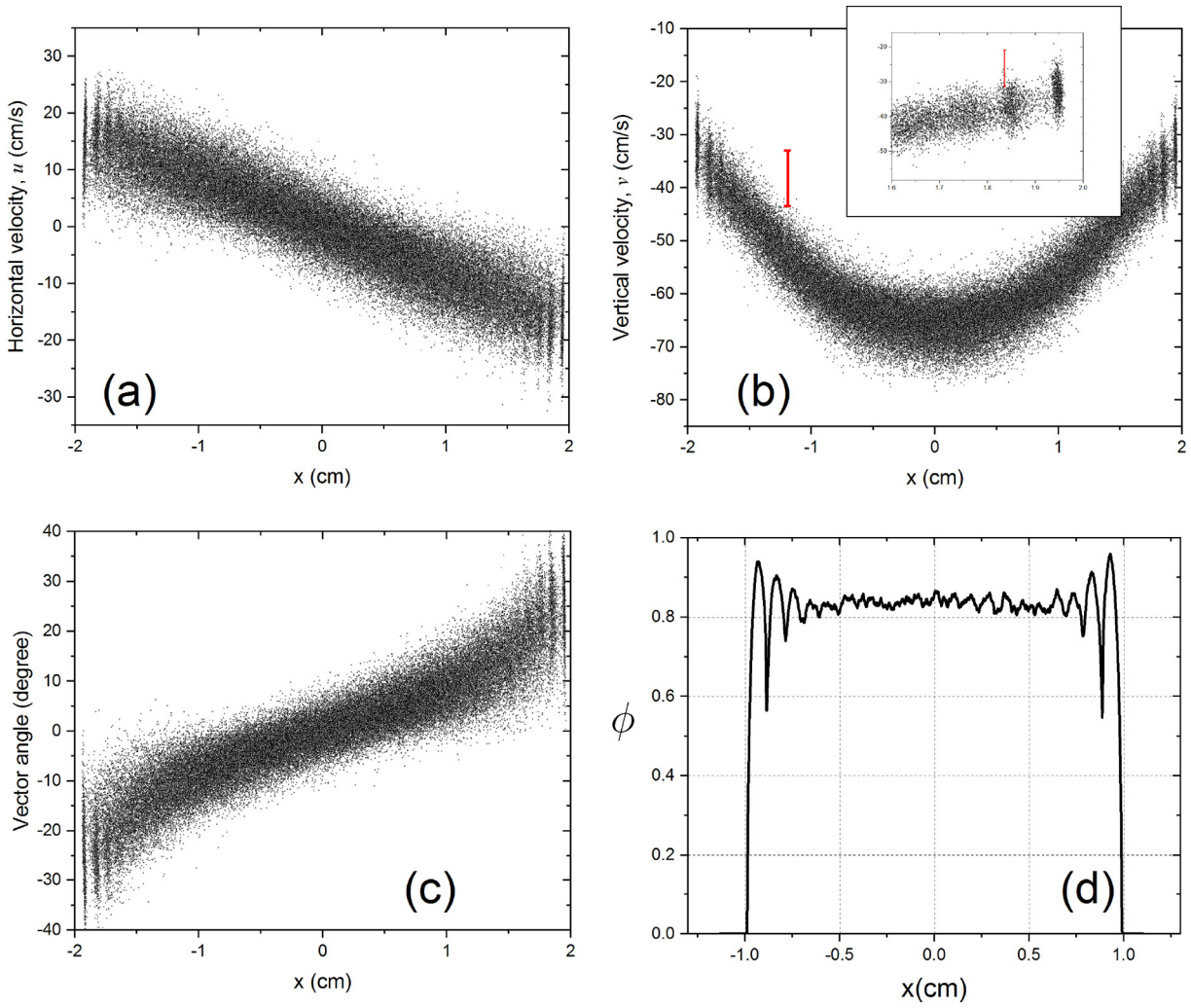

Fig. 2. Experimental results: Each dot corresponds to the particles' horizontal (a) and vertical (b) velocities and (c) its angular deviation. (d) 2D-solid-fraction profile. All the results correspond to the largest explored orifice, $R = 2.0cm$. The inset in (b) zooms the velocity values (including its typical error bar) near the outlet border.

The lateral sheets location also determines the silo width (280 bead diameters in the worst case) and sets the outlet aperture $D = 2R$ (Fig. 1.b). Note that we use the notation used in [8] for the slit span, setting the coordinate system origin at the centre of exit slit. An intense LED panel illuminates the outlet region from rear, while a high-speed camera (*FASTCAM Mini UX100*) with a macro lens is used to record videos from the front. Optical field of view was selected attending two crucial requirements: i) the spatial resolution necessary to measure the particle position with reasonable precision (around 25 pixels per millimeter) and ii) the need to explore a broad region near the exit orifice to characterize the fields in the outlet neighborhood. Also, to perform the beads tracking, it is crucial to guarantee that their displacement between two consecutive frames is smaller than half the particle diameter. This fact imposed a camera frame rate that reached 4000 *fps* in some cases. High shutter speed was also used (10^{-5} seconds) to prevent blur effects at the particles edges.

From the video images, a hand-made post-processing image protocol detects all the particle centroids which are used to calculate the velocity vectors with high accuracy. To estimate the experimental error, we neglect the temporal uncertainty which is around tens of nanosecond and assume the worst situation respect the spatial displacement; i.e. we consider that centroid displacements between two successive frames lies with equal probability in the interval fixed by the image discretization. Hence, the error bars indicated for all the velocity signals are given by the $[pixel\ length \cdot fps/\sqrt{3}]$ [16].

Along this paper, we will focus our analysis on the velocity exit, defined just at the outlet plane, $\mathbf{v}(z=0) \equiv \vec{e}_x u + \vec{e}_z v$. In the same way, we use the solid-fraction at $z = 0$, which is computed from the centroids positions and the radius of the particles using a simple trigonometric relationship. Finally, the calculated solid-fraction for each frame is then averaged over all frames registered. The flow rate is given by the number of particles passing through $z = 0$ divided by the period of observation. Typical experimental runs imply the registration of more than $4 \cdot 10^5$ centroids passing through the outlet.

3. Experimental results

3.1. Solid-fraction and velocity profiles

Let us start describing the kinematic variables near the outlet; i.e. the particles horizontal and vertical velocities, their alignment against the gravity direction and the exit solid-fraction profile. Fig. 2 shows a typical set of observations corresponding to the largest exit orifice studied ($D = 4.02 \pm 0.01$ cm) and a hopper angle, $\alpha = 60°$. Figs. 2.a,b display the horizontal, u, and vertical, v, velocity of $2 \cdot 10^5$ particles passing through the outlet. Despite some dispersion, both magnitudes display a high degree of symmetry around the orifice centre. Remarkably, both figures show that a good number of particles pass through the region adjacent to the orifice border (see inset of Fig. 2.b). It is also evident that the wall induces some degree of order due to the use of monodisperse beads. These observations agree with the results reported for flat bottomed silos and confirms that the idea of *empty annulus* or reduced effective orifice is unreal and must be considered as a vague approximation. Fig. 2.c reports the angular orientation of the velocity vectors (with respect to gravity), evidencing a large dispersion of this magnitude near the outlet border. A careful inspection of the high-speed movies revealed that many particles pass through this zone with an orientation almost parallel to the z-coordinate. All these results are coherent with the 2D-solid-fraction displayed in Fig. 2.d. Again, the signal oscillation near the border reflects the particle order. However, oscillations almost disappear when the distance from the outlet border increases, where the solid-fraction profile becomes almost flat. Note that even for this large exit aperture (around twenty particle diameters) the maximum of ϕ is slightly below the 2D bulk-solid-fraction ($\phi_B \approx 0.91$).

After describing the general features of the data obtained for the different explored parameters, let us analyze their dependence with the outlet size and the hopper angle. To this end, we concentrate on v and ϕ as these magnitudes determine the outlet volumetric flow-density, and consequently, the hopper flow rate. Fig. 3 shows the velocity profiles corresponding to $D \cong 2$ cm (small differences exist between the three values of D) and $\alpha = 60°$, 30° and 10° respectively. As can be appreciated from the figure, the hopper angle controls both, the velocity profiles shapes and the magnitude of this variable at the slit centre.

Two different relationships could be used to fit the data displayed in Fig. 3. The first one is the same expression used in [8,10]:

$$v_I(v_c, a) = v_c \cdot \left(1 - (x/R)^2\right)^a \tag{9}$$

where the exit velocity at the orifice centre, v_c, is a free fitting parameter and the profile shape is controlled by a. Although this expression reproduces very well the coarse-grained velocity profile, it imposes a vanishing velocity at the outlet border; clearly this fact is not true for the velocity in a hopper.

To solve this disagreement an alternative expression can be used extending the ideas introduced in [9]:

$$v_{II}(\gamma, a) = \sqrt{2g\gamma R} \cdot \left(1 - (x/\gamma R)^2\right)^a \tag{10}$$

Here, $v_c = \sqrt{2g\gamma R}$ depends on a length proportional to the outlet size, γR, that also controls the sliding velocity at the outlet border. In this equation γ is a free fitting parameter although their influence on v_c is justified by Eq. 6.

Fig. 3 evidences that both approaches predict basically the same coarse-grained profiles for all the experimental points, despite the expected disagreement for $x > R$. Furthermore, v_c is essentially the same

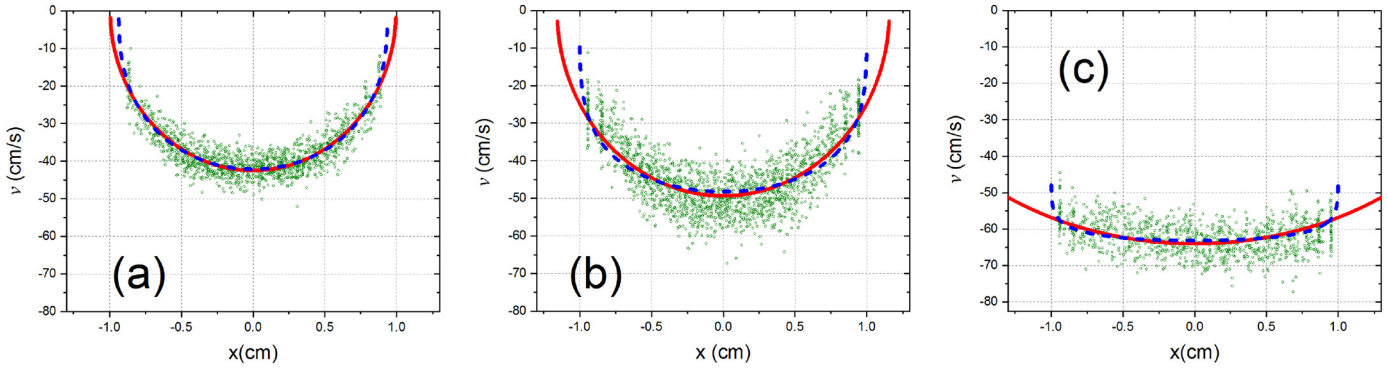

Fig. 3. Angular dependence of the exit velocity: Experimental data for (a) $\alpha = 60°$, (b) $\alpha = 30°$ and (c) $\alpha = 10°$. Only 10% of experimental results are displayed. Dashed and continuous lines correspond to the fittings of Eq. 9 and Eq. 10 respectively.

in both fittings (in the worst case, it differs less than 5%). For practical reasons, we use Eq. 9 to fit all the experimental data and obtain the corresponding values of v_c for the explored hopper angles and for all the outlet sizes investigated, $v_c(\alpha, R)$.

After this, we rescale the measured velocities by its corresponding v_c, and its x-coordinate by R as it was done in [8]. Applying this scaling, all the profiles obtained with the same hopper angle collapse, as shown in Fig. 4.(a-c). Therefore, a single expression can be used to describe the collapsed data for each hopper angle. Again, we check that using Eq. 9 or Eq. 10 has not a substantial impact on the profiles obtained (see lines in Fig. 4.(a-c)). Nevertheless, as we mentioned above, the use of one or another fitting function imply non-trivial consequences in its kinematic interpretation. Eq. 9 is conditioned by the requirement of having a null velocity when $x = R$, but does not provide any argument about the physical origin of v_c; on the contrary, Eq. 10 uses the factor γ to account for the acceleration profile in the vertical direction [9]; in addition, the fit quality suggests that γ controls the sliding velocity just at the hopper border. Finally, the exponent a sets the profile curvature, which is conditioned by the kinetic stress symmetry inside the bulk.

We harmonize both ideas fitting the values of v_c obtained from Eq. 9 with the expression $v_c(\alpha, R) = \sqrt{2g\gamma(\alpha)R}$ where a single value of $\gamma(\alpha)$ is considered as control parameter. As it is clear from Fig. 4.d, the fitting quality is good, except maybe for the smallest orifices when $\alpha = 10°$. Table 1 summarizes the parameter values used to fit the collapsed profiles for each hopper angle. Clearly, the smaller the hopper angle, the lower the values obtained for a implying a smoother (or less curved) profiles. Moreover, the different γ values obtained for each α indicates that the hopper angle controls the effective acceleration along the vertical direction.

Table 1
Values of the fitting coefficients used for the velocity and density profiles. The values of the flat bottom silo, $\alpha = 90°$, have been extracted from Ref. [8].

Hopper angle, α	γ	a	ϕ_∞	b
90°	1.07	0.50	0.84	0.25
60°	0.98	0.45	0.84	0.20
30°	1.18	0.28	0.86	0.05
10°	1.92	0.12	0.86	0.02

Let us now focus on the solid-fraction dependence on the hopper angle. Fig. 5 summarized the results for all the explored outlet sizes. One of the main conclusions that can be extracted is that all the profiles

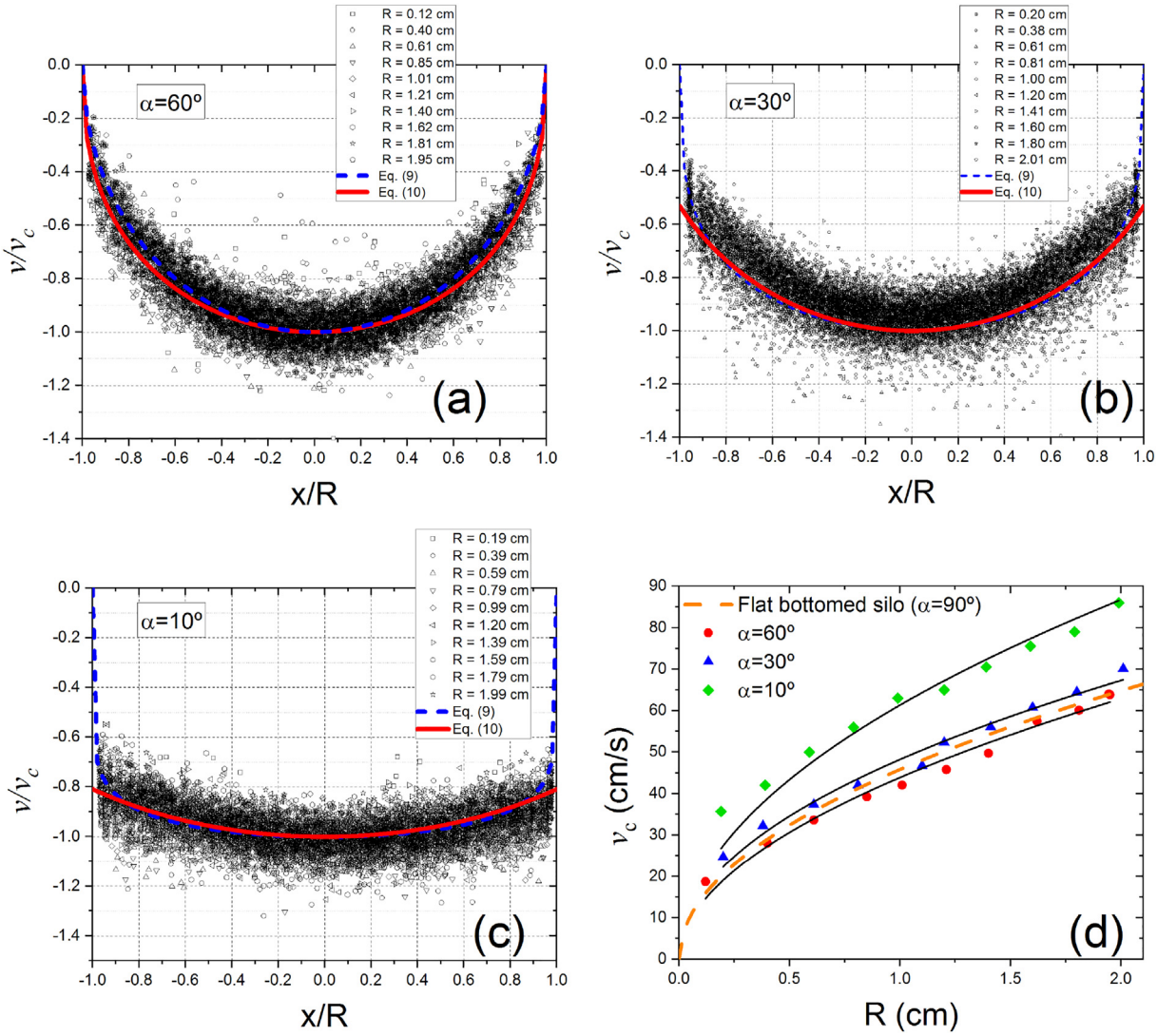

Fig. 4. Collapsed velocities profiles: Vertical velocity data obtained for several outlets when (a) $\alpha = 60°$, (b)$\alpha = 30°$ and (c) $\alpha = 10°$. Dashed and continuous lines correspond to the fitting functions v_I (Eq. 9) and v_{II}(*Eq.* 10) respectively. (d) Velocity at the outlet centre, v_c, as a function of the outlet radius R for the hopper angles indicated in the legend. Continuous lines correspond to $v_c(R) = \sqrt{2g\gamma R}$ using the γ values displayed in Table 1. The dashed line is the prediction introduced in [8] for a flat bottomed silo.

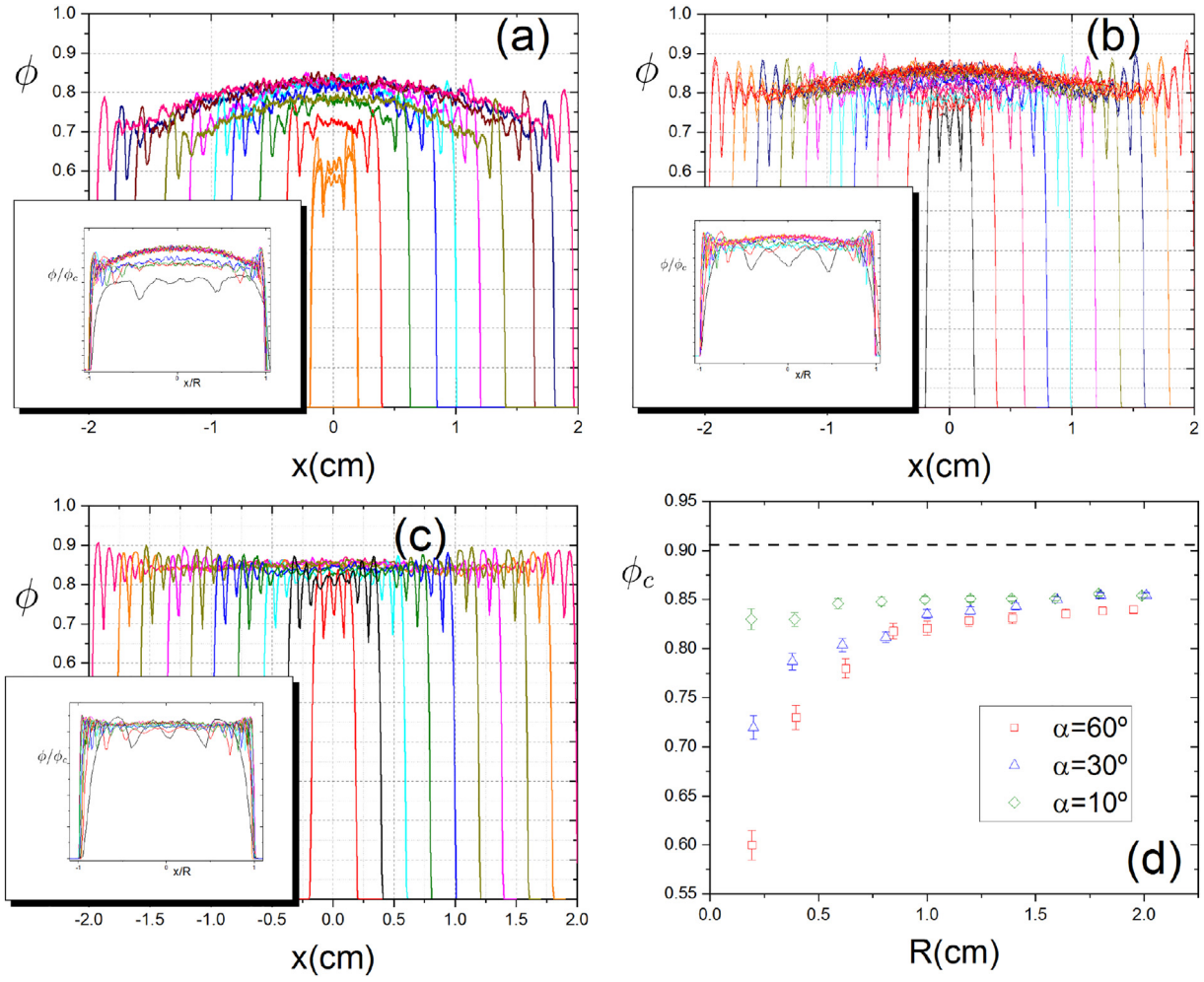

Fig. 5. 2D-solid-fraction profiles: The displayed data correspond to (a) $\alpha = 60^{\circ}$, (b) $\alpha = 30^{\circ}$ and (c) $\alpha = 10^{\circ}$ respectively. Insets display the normalized profiles. (d) 2D-solid-fraction at the outlet centre ϕ_c as a function of half the outlet size, R. Error bars of ϕ_c express the parameter uncertainty obtained from the fitting function (Eq. 11). Dotted line indicates the bulk solid-fraction limit, ϕ_B.

are less curved than those reported for a flat bottomed silo [8]. Like in that work, the solid-fraction profiles obtained for a given hopper angle can be collapsed normalizing $\phi(x)$ with ϕ_c (the 2D-solid-fraction at the orifice centre) and the x-coordinate with R (see the insets in Figs. 5.a-c). In the same way, the profiles can be fitted by the expression:

$$\phi(\phi_c, b) = \phi_c\left(1-(x/R)^2\right)^b \tag{11}$$

where b determines the profile shape. Provided that the scaled data collapse into a single functional dependence (except perhaps when exploring small apertures), we obtain for each hopper angle a single value for the parameter b (see Table 1). Note that the impact of this parameter on the discharge process is rather week as all the profiles displayed in Fig. 5 are almost flat.

The values of ϕ_c obtained using Eq. 11 for each experimental set are plotted in Fig. 5.d revealing that, in all cases, ϕ_c decreases when reducing R. This behavior, which can be attributed to the granular dilatancy when the material pass through small orifices, almost disappears when α is small. Indeed, when $\alpha = 10^{\circ}$ the difference among the maximum and minimum values of ϕ_c is only 1.6%. Moreover, Fig. 5.d also reveals that the asymptotic value of ϕ_c for large outlets, ϕ_∞, is only smoothly dependent on the hopper angle (see Table 1). In line with the arguments introduced in [8], ϕ_∞ falls always below the bulk solid-fraction (see dashed line in Fig. 5d). Hence, it is reasonable to assume from a practical point of view that $\phi_\infty \simeq 0.85$ independently of the hopper angle.

In summary, the data outlined in this section show that the hopper angle has a notable influence on the exit velocity as v_c raises when α is reduced. On contrary the influence on ϕ_c only becomes relevant for small R's, evolving to almost equal asymptotic values for large outlet sizes.

4. Flow rate implications

In this section, we will correlate the kinematic magnitudes described in the previous section with the volumetric flow rate, Q. First, let us compare the experimentally measured flow rates with the predicted ones using the fittings of Eqs. 3 and 4. To do that we represent $Q(R)$ versus R in Fig. 6, where we also include the $\alpha = 90^{\circ}$ results reported in [8]. A rapid inspection of the data shows that the flow rate corresponding to $\alpha = 60^{\circ}$ is slightly below the one obtained for $\alpha = 90^{\circ}$. This observation, although implicit in the expression introduced by Brown and Richards (Eq. 8), has been experimentally evidenced in a single work [10]. Beyond this, all the measured flow rates follow the expected nonlinear growth with $R^{3/2}$ as it is clear from Fig. 6.b, where $Q^{2/3}$ is plotted versus R. To understand the physics behind this result and analyze the way in which the reported profiles determine Q, let us introduce the volumetric flow-density vector, $\vec{J}$, defined as:

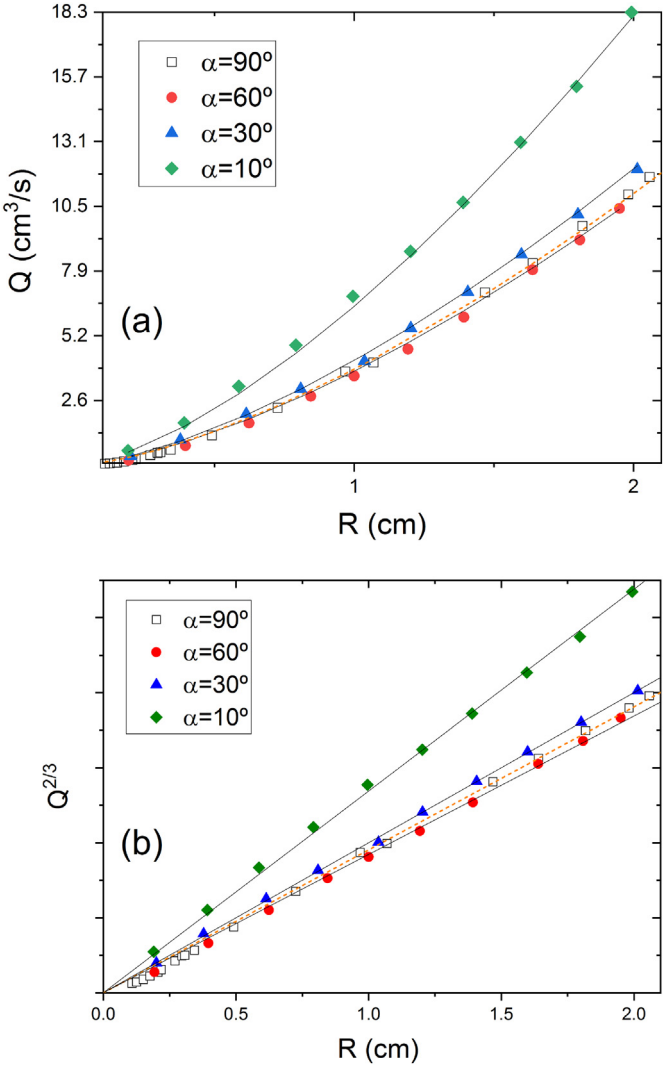

Fig. 6. Volumetric flow rates: (a) Measured for different hopper angles, including the one corresponding to $\alpha = 90^{\circ}$ extracted from [8], as indicated in the legend. (b) The same values are displayed with a nonlinear abscissa. In both graphs, continuous lines correspond to the flow rates predicted by Eq. 15 using the parameters reported in Table 1 and dashed lines to the fitting proposed in [8] for a flat bottomed silo.

$$\vec{J}(x,z) = -\vec{e}_z \frac{2}{3}\phi(x,z)\ v(x,z) \tag{12}$$

where $\frac{2}{3}\phi(x,z)$ is the volumetric fraction corresponding to a mono-layer of spheres with a 2D solid-fraction, $\phi(x,z)$. Hence, assuming that Eqs. 3 and 4, are representative of $v(x,z=0)$ and $\phi(x,z=0)$, the volumetric flow rate can be written as:

$$Q = \int \vec{J}(x,z=0)\cdot \vec{d}A = \frac{2}{3}\phi_c v_c \int_{-r}^{r}\int_{-R}^{R}\left[1-(x/R)^2\right]^{a+b} dxdy \tag{13}$$

After integrating,

$$Q = \beta\left(\frac{1}{2}, 1+[a+b]\right)\frac{2}{3}\phi_c v_c\, dR \tag{14}$$

Finally, using $v_c = \sqrt{2g\gamma R}$ we obtain:

$$Q(R,\alpha) = \frac{2\sqrt{2}}{3}\beta\left(\frac{1}{2}, 1+[a+b]\right)\sqrt{\gamma g}\,\phi_c\, dR^{3/2} \tag{15}$$

Note that eq. 15 -like the one introduced for the flow rate in the sixties- contains two parameters relating particle kinematics with the silo discharge rate. These parameters account for: (a) the profiles shape through the β-function, and (b) the vertical acceleration through the γ factor. As $\beta\left(\frac{1}{2}, 1+[a+b]\right)$ is a smooth non-linear function of $a+b$, small changes in the curvature profiles have a weak impact in Q. On the contrary, as γ controls the discharge velocity, it becomes the main magnitude behind the flow rate increment when modifying the hopper angle. Continuous lines depicted in Fig. 6 correspond to the calculated flow rate using the $[a+b]$ and γ values introduced in Table 1. Importantly, ϕ_c is replaced by ϕ_∞ assuming that we are interested in the limit of large outlet sizes (see Table 1). The agreement seems to be excellent as it is also corroborated when representing $Q^{2/3}$ versus R. Nevertheless, some deviations exist for low values of the outlet size, mainly due to the approximation made when using ϕ_∞.

To unmask the hopper angle role we compare the former results with the flow rate obtained in a flat bottomed silo in the case of large apertures, Q_{90°. As depicted in Fig. 6, the predicted flow rate can be calculated replacing the parameter values introduced by Janda *el al.* [8] in Eq. 15 which then reads as:

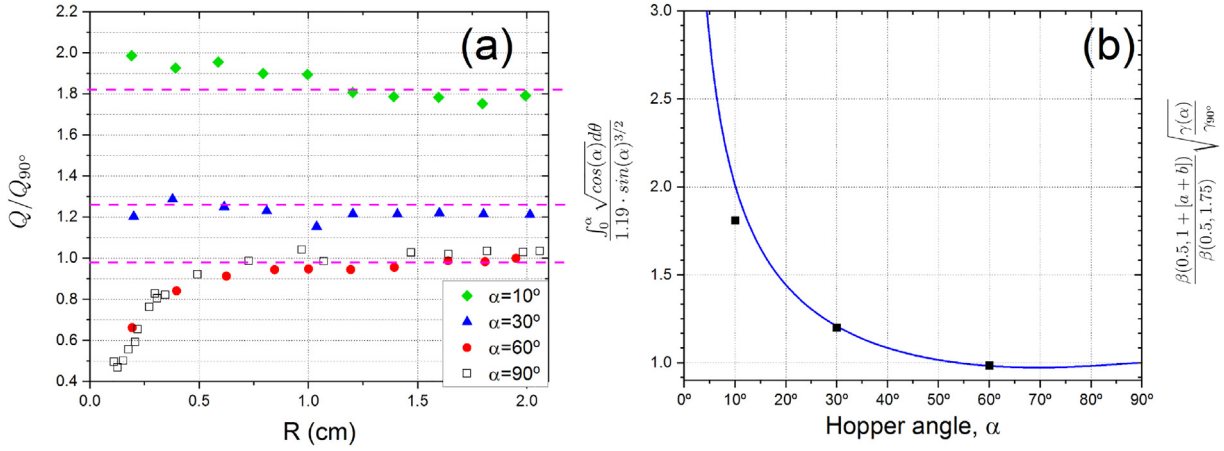

Fig. 7. Normalized flow rates: (a) Experimental flow rates normalized with the prediction introduced for flat bottomed silos (Eq. 16). Dashed lines correspond to the values obtained from Eq. 17. (b) The same factor but using the expression proposed by Brown and Richards normalized by its corresponding value for $\alpha = 90^{\circ}$ (see Eq. 18). Square dots indicate the values of the dashed lines in (a). (For interpretation of the references to colour in this figure legend, the reader is referred to the web version of this article.)

$$Q_{90^\circ} = \frac{2\sqrt{2}}{3}\beta\left(\frac{1}{2}, 1, 75\right)\sqrt{1.07g}0.8450.1, R^{3/2} \quad (16)$$

assuming that $\phi_c = \phi_\infty \simeq 0.845$.

Once Q_{90° is obtained, we use it to normalize the experimental flow rates obtained for different hopper angles (see Fig. 7a). We can extract a few relevant remarks from this figure. The first one is that Eq. 15 does not adequately fit the experimental data corresponding to small orifices, as it was expected when using ϕ_∞ to calculate Q_{90°. In this region, the flow is below the expected value $Q/Q_{90^\circ} = 1$, and reduces until $Q/Q_{90^\circ} = 0.5$ for the smallest explored aperture. Nevertheless, this effect disappears when reducing α as the normalized flow rate remains almost constant independently on R. Clearly, this feature correlates with the dependence of the solid-fraction with R for low hopper angles (see Fig. 5.d). Hence, disregarding the small differences in the asymptotic solid-fraction ϕ_∞, we obtain:

$$Q(\alpha)/Q_{90^\circ} = \frac{\beta(0.5, 1 + [a(\alpha) + b(\alpha)])}{\beta[0.5, 1.75]}\sqrt{\frac{\gamma(\alpha)}{\gamma_{90^\circ}}} \quad (17)$$

The outcomes of this expression (using the coefficients reported in Table 1), and the corresponding ones for the flat bottomed case are represented by horizontal dashed lines in Fig. 7.a. The data reveal a good agreement for large outlet sizes and stress, one more time, the inability of Eq. 16 to reproduce the flow rates obtained for small outlets. Nevertheless, the normalized flows emphasize how the hopper angle affects the vertical exit velocity (through γ parameter) and, in a lesser degree, the resulting velocity-volume-fraction profile shape encompassed into the β-function. Indeed, whereas the $\sqrt{\gamma(10^\circ)/\gamma_{90^\circ}} \simeq 1.4$, $\beta(\alpha = 10°)/\beta(\alpha = 90°) \simeq 1.28$. The normalization strategy leading to Eq.17 can be also implemented for the Brown and Richards' expression (Eq. 8). In that case, the multiplicative factor accounting for the angular dependence is:

$$Q^{BR}(\alpha)/Q^{BR}_{90^\circ} = \frac{\int_0^\alpha \sqrt{cos(\alpha)}d\theta}{1.19 \cdot \ sin(\alpha)^{3/2}} \quad (18)$$

This magnitude has been calculated and represented versus α in Fig. 7.b. In the graph, experimental flow ratios corresponding to the different hopper angles have also been included revealing an excellent agreement between both approaches. Hence, although the formal relation between velocity and solid-fraction profiles is not evident from the experimental data, it is conceivable than the flow-density introduced to obtain Eq.15 comprise, indeed, the symmetry arguments used by Brown and Richards in Eq. 18. Such a possibility will be explored in future research.

5. Concluding remarks

In this work, we have shown that the velocity and solid-fraction profiles at the exit of a 2D hopper display the same self-similarity properties reported for a flat bottom silo. Both profiles contribute to the flow rate equation with measurable parameters having a well defined physical meaning. Our measurements reveal that the hopper angle effect in the velocity profiles (Fig. 4) is both qualitative (the profiles flatten when α reduces) and quantitative (the maximum velocity at the centre of the outlet increases when α decreases). The latter effect becomes more pronounced for large values of R. Moreover, reducing the hopper angle also leads to flatter solid-fraction profiles. However, in this case the magnitude of the solid fraction at the outlet center asymptotically tends to a value which does not seem to depend on the hopper angle. Then disparity of solid fraction for different α's only occurs for small R, becoming negligible for sufficiently large orifices.

All these effects can be linked with the flow-density vector $\vec{J}(x, y)$ through a set of parameters (ϕ_c, γ and $[a + b]$), that determine its magnitude. Accordingly, the assumption that the stress distribution imposed by the hopper angle drives the discharge rate is straightforward. Such idea introduced in a simplified way by Brown [1] in the postulate of "Minimum Energy", seems to be related with our approach through the spatial distribution of $\vec{J}(x, y)$. Thus, the *free fall arch* paradoxical conditions at the dome where a sudden jump occurs in the particles acceleration [17], can be replaced by the smooth evolution of the vertical acceleration described by Rubio-Largo et al. in [9]. In this work, we show that the γ parameter, which must be connected with the vertical acceleration, is influenced by the hopper angle. In this regard, the outcomes of this work are in good agreement with the flow rate dependence on the particle size reported in [18] where the formation of a dead zone near the outlet is suggested to act as an induced natural hopper.

Let us finally note that the kinematic variables studied in the preceding sections provide an unambiguous way to calculate the mass flow rate for all hopper angles. In fact, a compact version of the Eq. 15 could be condensed as:

$$Q = C(\alpha)\phi_c\sqrt{\gamma(\alpha)g}R^{3/2} \quad (19)$$

Now, the parameters included in the equation are explained by (a) the influence of the radial symmetry of the profiles through $C(\alpha)$; (b) the material dilatancy near the outlet ϕ_c; and (c) the dependence of the particle acceleration with the hopper angle $\gamma(\alpha)$. The above results seem to point out that it should be possible to relate the formalism introduced by Brown & Richards with the stress field symmetry within the silo, which, indeed, controls the parameters described above. Finally, it is evident that the empiric parameter k introduced en Eq. 1 is unnecessary when using a coarse-grained approach as the introduced in this work.

Declaration of Competing Interests

The authors declare that they have no known competing financial interests or personal relationships that could have appeared to influence the work reported in this paper.

Acknowledgments

This work was partially funded by Universidad de Navarra and Ministerio de Economía y Competitividad (Spanish Government) through Project No. FIS2017-84631 MINECO/AEI/FEDER,UE.

References

[1] R.L. Brown, Minimum energy theorem for flow of dry granules through apertures, Nature 191 (1961) 458–461, https://doi.org/10.1038/191458a0. URL. https://doi.org/10.1038/191458a0.
[2] T. Knowlton, G. Klinzing, W. Yang, J. Carson, The importance of storage, transfer, and collection, Chemical Engineering Progress; (United States), 90, 1994 4.
[3] W. Beverloo, H. Leniger, J. van de Velde, The flow of granular solids through orifices, Chem. Eng. Sci. 15 (3) (1961) 260–269, https://doi.org/10.1016/0009-2509(61)85030-6. http://www.sciencedirect.com/science/article/pii/0009250961850306.
[4] B.P. Tighe, M. Sperl, Pressure and motion of dry sand: translation of hagen's paper from 1852, Granul. Matter 9 (2007) 141–144, https://doi.org/10.1007/s10035-006-0027-x.
[5] R.M. Nedderman, Statics and Kinematics of Granular Materials, Cambridge University Press, 1992https://doi.org/10.1017/CBO9780511600043.
[6] R. Brown, J. Richards, Principles of Powder Mechanics, Pergamon, 1970https://doi.org/10.1017/CBO9780511600043.
[7] C. Mancok, A. Janda, R. Arévalo, J.M. Pastor, I. Zuriguel, A. Garcimartn, D. Maza, The flow rate of granular materials through an orifice, Granul. Matter 9 (2007) 407, https://doi.org/10.1007/s10035-007-0062-2. URL. https://doi.org/10.1007/s10035-007-0062-2.
[8] A. Janda, I. Zuriguel, D. Maza, Flow rate of particles through apertures obtained from self-similar density and velocity profiles, Phys. Rev. Lett. 108 (2012) 248001, https://doi.org/10.1103/PhysRevLett.108.248001. URL. https://link.aps.org/doi/10.1103/PhysRevLett.108.248001.

[9] S.M. Rubio-Largo, A. Janda, D. Maza, I. Zuriguel, R.C. Hidalgo, Disentangling the free-fall arch paradox in silo discharge, Phys. Rev. Lett. 114 (2015) 238002, https://doi.org/10.1103/PhysRevLett.114.238002. URL. https://link.aps.org/doi/10.1103/PhysRevLett.114.238002.

[10] B. Mebirika, P. Aussillous, B. Dalloz-Dubrujeaud, Discharge flow of a granular media from a silo: effect of the packing fraction and of the hopper angle, EPJ Web of Conferences 140 (2017), 03043. https://doi.org/10.1051/epjconf/201714003043.

[11] S.M. Rubio-Largo, D. Maza, R.C. Hidalgo, Large-scale numerical simulations of polydisperse particle flow in a silo, Computational Particle Mechanics 4 (4) (2017) 419–427, https://doi.org/10.1007/s40571-016-0133-4. URL. https://doi.org/10.1007/s40571-016-0133-4.

[12] M. Madrid, K. Asencio, D. Maza, Silo discharge of binary granular mixtures, Phys. Rev. E 96 (2017), 022904. https://doi.org/10.1103/PhysRevE.96.022904. URL. https://link.aps.org/doi/10.1103/PhysRevE.96.022904.

[13] K. Saleh, S. Golshan, R. Zarghami, A review on gravity flow of free-flowing granular solids in silos basics and practical aspects, Chem. Eng. Sci. 192 (2018) 1011–1035, https://doi.org/10.1016/j.ces.2018.08.028. URL. http://www.sciencedirect.com/science/article/pii/S0009250918305979.

[14] D. López-Rodríguez, D. Gella, K. To, D. Maza, A. Garcimartín, I. Zuriguel, Effect of hopper angle on granular clogging, Phys. Rev. E 99 (2019), 032901. https://doi.org/10.1103/PhysRevE.99.032901. URL. https://link.aps.org/doi/10.1103/PhysRevE.99.032901.

[15] T.V. Nguyen, C. Brennen, R. Sabersky, Gravity flow of granular materials in conical hoppers, J. Appl. Mech. 46 (1979) 529, https://doi.org/10.1115/1.3424601.

[16] J. C. for Guides in Metrology, Jcgm 100: Evaluation of measurement data - guide to the expression of uncertainty in measurement, Tech. rep., JCGM (2008). https://www.iso.org/sites/JCGM/GUM-JCGM100.htm.

[17] R. Nedderman, U. Tzn, S. Savage, G. Houlsby, The flow of granular materialsi: discharge rates from hoppers, Chem. Eng. Sci. 37 (11) (1982) 1597–1609, https://doi.org/10.1016/0009-2509(82)80029-8. http://www.sciencedirect.com/science/article/pii/0009250982800298.

[18] D. Gella, D. Maza, I. Zuriguel, Role of particle size in the kinematic properties of silo flow, Phys. Rev. E 95 (2017), 052904. https://doi.org/10.1103/PhysRevE.95.052904. URL. https://link.aps.org/doi/10.1103/PhysRevE.95.052904.